# Timing Ultra-Wideband Signals With Dirty Templates

Liuqing Yang, *Member, IEEE,* and Georgios B. Giannakis, *Fellow, IEEE*

***Abstract*—Ultra-wideband (UWB) technology for indoor wireless communications promises high data rates with low-complexity transceivers. Rapid timing synchronization constitutes a major challenge in realizing these promises. In this paper, we establish a novel synchronization criterion that we term "timing with dirty templates" (TDT), based on which we develop and test timing algorithms in both data-aided (DA) and nondata-aided modes. For the DA mode, we design a training pattern, which turns out to not only speed up synchronization, but also enable timing in a multiuser environment. Based on simple integrate-and-dump operations over the symbol duration, our TDT algorithms remain operational in practical UWB settings. They are also readily applicable to narrowband systems when intersymbol interference is avoided. Simulations confirm performance improvement of TDT relative to existing alternatives in terms of mean square error and bit-error rate.**

***Index Terms*—Direct sequence (DS), estimation and detection, multipath, synchronization, time-hopping (TH), timing acquisition, tracking, ultra-wideband (UWB).**

## I. Introduction

SINCE the Federal Communications Commission's Record and Order commercializing ultra-wideband (UWB) systems in February 2002, UWB radios have attracted increasing interest, thanks to their potential to offer high user capacity with low-complexity, low-power transceivers; see, e.g., [4], [18], [21], and references therein. One of the most critical challenges in enabling the unique benefits of UWB radios is the synchronization step (a.k.a. timing offset estimation). Information-theoretic studies corroborate that the achievable mutual information in the UWB regime hinges heavily upon accurate timing information [11]. Bit-error rate (BER) analysis also reveals pronounced performance degradation of UWB radios due to mistiming [14].

Though synchronization is also a challenge in narrowband systems, its difficulty is accentuated in UWB due to the fact that the information-bearing waveforms are impulse-like and have low power. Moreover, the (oftentimes dense) multipath channel, through which these low-power narrow pulses propagate, is unknown at the receiver during the synchronization stage. These reasons explain why synchronization has received so much emphasis in UWB research [2], [8], [10], [15], [22]. However, each of these approaches requires one or more of the following assumptions: 1) multipath is absent; 2) time-hopping (TH) codes are slow or even absent; 3) the multipath channel is known; and 4) the system can afford the prohibitive complexity of exhaustively searching over thousands of bins (chips). Evidently, timing algorithms based on these assumptions are impractical for most realistic UWB settings.

In this paper, we will develop timing algorithms without invoking any of the aforementioned assumptions. Our timing algorithms remain operational in general UWB settings with TH and/or direct-sequence (DS) spreading, *unknown* multipath propagation, and even when multiple (and possibly asynchronous) users are present. Unlike existing alternatives, our synchronizers rely on symbol-rate samples, and thus entail low complexity. Equally attractive is the fact that their applicability is not confined to UWB applications. They can be readily applied to narrowband, wideband, single- or multiuser systems, as long as intersymbol interference (ISI) is avoided.

Our timing algorithms rely on a novel synchronization criterion. Most existing synchronizers are based on the unique maximum of the received pulse's autocorrelation function, which requires a "clean template" of the received pulse to be available. Evidently, the latter is not feasible when the multipath channel is unknown. Our novel criterion relies on the fact that the cross correlation of "dirty templates" extracted from the received waveform exhibits a unique maximum at the correct timing. These dirty templates we will introduce in the ensuing sections render channel information unnecessary at the synchronization stage, since it is embedded in the received waveform. The resultant algorithm, that we will term "timing with dirty templates" (TDT), not only achieves timing, but also improves acquisition performance over competing alternatives by collecting the rich multipath energy provided by UWB channels.

Similar to the transmitted reference (TR) approaches for symbol demodulation [7], our TDT algorithms require simple integrate-and-dump operations at the symbol rate. But different from TR, which relies on 50% training (pilot) symbols, our TDT algorithms entail no or a small number of training symbols. While TR requires timing to operate, our TDT algorithms are designed in order to acquire timing synchronization.

The rest of the paper is organized as follows. Section II outlines our system model and operating transceiver conditions. Section III introduces our novel synchronization criterion and (non)data-aided variants of the TDT algorithm in a single-user

Paper approved by S. N. Batalama, the Editor for Spread Spectrum and Estimation of the IEEE Communications Society. Manuscript received June 11, 2004; revised February 20, 2005 and May 11, 2005. This work was prepared through collaborative participation in the Communications and Networks Consortium sponsored by the U.S. Army Research Laboratory under the Collaborative Technology Alliance Program, Cooperative Agreement DAAD19-01-2-0011, and was supported in part by the National Science Foundation under Grant EIA-0324864. This paper was presented in part at the GLOBECOM Conference, San Francisco, CA, December 2003, and in part at the International Conference on Acoustics, Speech, and Signal Processing, Montreal, QC, Canada, May 2004. The U.S. Government is authorized to reproduce and distribute reprints for Government purposes notwithstanding any copyright notation thereon.

L. Yang is with the Department of Electrical and Computer Engineering, University of Florida, Gainesville, FL 32611 USA (e-mail: lqyang@ece.ufl.edu).

G. B. Giannakis is with the Department of Electrical and Computer Engineering, University of Minnesota, Minneapolis, MN 55455 USA (e-mail: georgios@ece.umn.edu).

Digital Object Identifier 10.1109/TCOMM.2005.858663

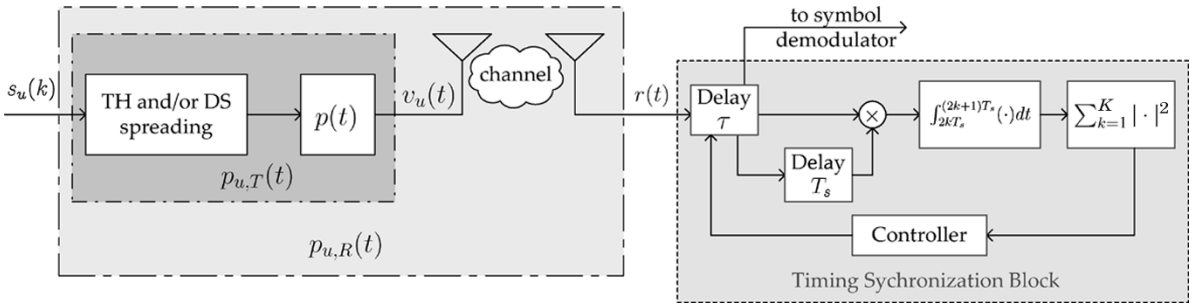


Fig. 1. Block diagram of the UWB transmitter and receiver. Synchronization block shown is for *Propositions 1* and *2*.

link. Performance of these algorithms is analyzed, and comparisons are provided in Section IV. The single-user TDT algorithms are generalized to multiuser settings in Section V. Simulations and numerical results are presented in Section VI, while concluding remarks are given in Section VII.

*Notation:* $\lceil\cdot\rceil$ and $\lfloor\cdot\rfloor$ stand for integer ceiling and floor operations, respectively; $\mathrm{E}\{\cdot\}$ and $\mathrm{var}\{\cdot\}$ represent expectation and variance operations; $[A]_B$ denotes the modulo operation with base $B$, where $A$ and $B$ are both real.

## II. Modeling and Preliminaries

In UWB impulse-radio multiple access, every information symbol is transmitted over a time interval of $T_s$ seconds that consists of $N_f$ frames, each of duration $T_f$. During each frame, a data-modulated ultra-short pulse $p(t)$, that has duration $T_p \ll T_f$, is transmitted. With pulse-amplitude modulation (PAM), the $k$th symbol from the $u$th user $s_u(k)$ is drawn equiprobably from a finite alphabet, and is energy normalized so that $\mathrm{E}\{s_u^2(k)\} = 1$. User separation is accomplished with pseudo-random DS and/or TH codes, which time-shift the pulse position at multiples of the chip duration $(T_c)$ [18]. After TH or DS spreading and pulse shaping by $p(t)$, as shown in Fig. 1, the transmitted waveform from the $u$th user is

$$v_u(t) = \sqrt{\mathcal{E}_u}\sum_{k=0}^{+\infty} s_u(k)p_{u,T}(t - kT_s)$$

where $\mathcal{E}_u$ is the energy per pulse, and $p_{u,T}(t)$ denotes the *transmitted* symbol waveform

$$p_{u,T}(t) := \sum_{n=0}^{N_f-1} p\left(t - nT_f - c_u(n)T_c\right)$$

containing $N_f$ pulses, shifted by the user-specific TH code $c_u(n)$ during the $n$th frame.

The multipath channel corresponding to each user $u$ is modeled as a tapped-delay line with $(L_u + 1)$ taps, whose amplitudes $\{\alpha_{u,l}\}_{l=0}^{L_u}$ and delays $\{\tau_{u,l}\}_{l=0}^{L_u}$ satisfy $\tau_{u,0} = 0$ and $\tau_{u,l} < \tau_{u,l+1}\ \forall l$. The channel is assumed to be quasi-static; i.e., $\{\alpha_{u,l}, \tau_{u,l}\}_{l=0}^{L_u}$ remain invariant over one transmission burst, but they are allowed to change independently from burst to burst. With the receiver frontend acting as an ideal bandpass filter with ultra-wide bandwidth $B$ centered at frequency $f_0$, the aggregate waveform from all users at the receive-filter output is

$$r(t) = \sum_{u=0}^{N_u-1}\sqrt{\mathcal{E}_u}\sum_{l=0}^{L_u}\alpha_{u,l}v_u(t - \tau_{u,l} - \tau_u) + \eta(t) \qquad (1)$$

where $N_u$ is the total number of active users, $\tau_u$ is the propagation delay of the $u$th user's direct path, and $\eta(t)$ is the bandpass-filtered zero-mean additive Gaussian noise (AGN) with power spectral density (PSD) $N_0/2$. Notice that by denoting multipath delays $\tau_{u,l}$ relative to the first arriving pulse, the propagation delay $\tau_u$ is decoupled from the dispersive effects of the multipath channel. The overall *received* symbol-long waveform capturing the pulse shaper, the dispersive channel effects, and the receive filter, is thus given by (see also Fig. 1)

$$p_{u,R}(t) := \sum_{l=0}^{L_u}\alpha_{u,l}p_{u,T}(t - \tau_{u,l}) \quad \forall u \in [0, N_u - 1]. \qquad (2)$$

To develop our TDT algorithms, we assume:

**(as)** the nonzero support of waveform $p_{u,R}(t)$ is upper bounded by the symbol duration $T_s$.

This assumption implies that ISI is absent, but allows interpulse and interframe interference to be present. In low-duty-cycle UWB systems, **(as)** is satisfied by choosing $T_f \geq \tau_{L,0} + T_p$ and $c_u(N_f - 1) = 0$; whereas in high-rate UWB radios, the condition $T_f \geq \tau_{L,0} + T_p$ can be relaxed as long as guard frames are inserted between symbols to avoid ISI, much like zero-padding in narrowband systems [16].

Using (2), the received waveform in (1) can be re-expressed as

$$r(t) = \sum_{u=0}^{N_u-1}\sqrt{\mathcal{E}_u}\sum_{k=0}^{+\infty} s_u(k)p_{u,R}(t - kT_s - \tau_u) + \eta(t). \qquad (3)$$

Next, we will develop a low-complexity approach that finds the desired user's timing offset $\tau_u$. Our synchronizer will be shown to be operational in a nondata-aided (NDA) (blind) mode, without knowledge of the multipath channel and the transmitted sequence. We will also show that with a judiciously designed training pattern, the data-aided (DA) mode of this synchronizer can further speed up timing acquisition, as well as improve synchronization and demodulation performance.

## III. TDT for Point-to-Point Links

In this section, we will focus on a single-user link and treat multiuser interference (MUI) as noise. After dropping the user index for notational brevity, the received waveform simplifies to [c.f. (1)]

$$r(t) = \sqrt{\mathcal{E}}\sum_{k=0}^{+\infty} s(k)p_R(t - kT_s - \tau_0) + \eta(t). \qquad (4)$$

Our idea for estimating $\tau_0$ hinges upon pairs of successive symbol-long segments of $r(t)$ taken at candidate time shifts $\tau \in [0, T_s)$, where one segment in each pair serves as template for the other. Specifically, integrate-and-dump operations are performed on products of such segments to obtain *symbol-rate* samples

$$x(k;\tau) = \int_0^{T_s} r(t+2kT_s+\tau) r\left(t+(2k-1)T_s+\tau\right) dt \quad \forall k \in [1,+\infty), \tau \in [0,T_s). \quad (5)$$

The symbol-long segments $r(t+2kT_s+\tau)$ and $r(t+(2k+1)T_s+\tau)$ for $t \in [0,T_s)$ serve as "templates" for each other in the correlation operation in (5). We call these templates "dirty" because: 1) they are noisy; 2) they are distorted by the *unknown* channel; and 3) they are subject to the *unknown* offset $\tau_0$. The latter constitutes a major difference between our TDT and the TR approach [7], which requires knowledge of $\tau_0$ beforehand to perform symbol demodulation. To grasp the gist of TDT, let $\chi(k;\tau)$ and $\rho(t)$ denote the noise-free parts of $x(k;\tau)$ and $r(t)$. Applying the Cauchy–Schwartz inequality to (5) yields

$$\chi^2(k;\tau) \le \int_0^{T_s} \rho^2(t+2kT_s+\tau)dt \int_0^{T_s} \rho^2\left(t+(2k-1)T_s+\tau\right)dt \quad (6)$$

where the equality holds $\forall k$ if and only if (iff) $\rho(t+2kT_s+\tau) = \lambda\rho(t+(2k-1)T_s+\tau)$, and $\lambda$ is an arbitrary scalar. But when does the latter hold true? Let us start with the explicit expression [c.f. (4)]

$$\rho(t+kT_s+\tau) = \sqrt{\mathcal{E}} \sum_{n=0}^{+\infty} s(n) p_R(t+kT_s+\tau-nT_s-\tau_0) \quad \forall t,\tau \in [0,T_s). \quad (7)$$

Since $p_R(t)$ has finite nonzero support $[0,T_s)$, the number of $n$ values that contribute nonzero summands in (7) must also be finite. Indeed, we prove in Appendix I that (7) simplifies to

$$\rho(t+kT_s+\tau) = \sqrt{\mathcal{E}} \sum_{m=0}^{1} s\left(k-k_{\tau_0}-m\right) p_R(t+mT_s-\tilde{\tau}_0) \quad (8)$$

$\forall t,\tau \in [0,T_s)$, where $k_{\tau_0} := \lfloor(\tau_0-\tau)/T_s\rfloor$ and $\tilde{\tau}_0 := [\tau_0-\tau]_{T_s}$. By definition, the integer $k_{\tau_0}$ can be either 0 or $-1$. Although it can induce delay in symbol demodulation, $k_{\tau_0}$ does not affect timing-offset estimation. For notational brevity, we will drop it hereafter. Equation (8) then becomes

$$\rho(t+kT_s+\tau) = \sqrt{\mathcal{E}}\, s(k-1) p_R(t+T_s-\tilde{\tau}_0) + \sqrt{\mathcal{E}}\, s(k) p_R(t-\tilde{\tau}_0) \quad \forall t,\tau \in [0,T_s). \quad (9)$$

For the condition $\rho(t+2kT_s+\tau) = \lambda\rho(t+(2k-1)T_s+\tau)$ to hold $\forall k$ and $\forall t \in [0,T_s)$, the following is required: $s(2k) = \lambda s(2k-1) = \lambda^2 s(2k-2)\,\forall k$. For a generic $\tilde{\tau}_0$, the latter holds true iff all odd indexed symbols are the same (say, $a$), and all even indexed symbols are $\pm a$, with $\lambda = 1$ if the two groups are the same, and $\lambda = -1$ otherwise. However, if $\tilde{\tau}_0 = 0$ (that is, $\tau = \tau_0$), then $p_R(t+T_s-\tilde{\tau}_0)$ vanishes, and the resultant $\rho(t+kT_s+\tau) = \sqrt{\mathcal{E}} s(k) p_R(t)$ ensures $\rho(t+2kT_s+\tau) = \lambda\rho(t+(2k-1)T_s+\tau)$ when PAM is used. Therefore, the equality in (6) holds for any sequence of information symbols, propagation channel (or equivalently, $p_R(t)$), and TH codes, iff $\tau = \tau_0$.[1]

In words, the cross correlation of successive symbol-long noise-free received segments reaches a *unique maximum* iff these segments are scaled versions of each other, which is achieved only at the correct timing; i.e., when $\tau = \tau_0$. In its simplicity, this observation offers a distinct criterion for timing synchronization, which for years has relied on the idea that the autocorrelation of the noise-free, known, and offset-free template has a unique maximum at the correct timing; the latter has been the principle behind all existing narrowband and UWB timing schemes, including the popular early–late gate algorithm [12]. The TDT approach is different from these conventional synchronizers. It has fundamental implications to UWB and also to a number of other applications, such as timing asynchronous code-division multiple-access (CDMA) transmissions and time-delay estimation through unknown time-dispersive media, where there is no undistorted template to rely on, even in the noise-free case.

To establish the validity of TDT in the presence of noise, let us start with the symbol-rate samples $x(k;\tau)$ [c.f. (5) and (9)]

$$x(k;\tau) = s(2k-1)\left[s(2k-2)\mathcal{E}_A(\tilde{\tau}_0) + s(2k)\mathcal{E}_B(\tilde{\tau}_0)\right] + \zeta(k;\tau) \quad (10)$$

where $\mathcal{E}_A(\tau) := \mathcal{E}\int_{T_s-\tau}^{T_s} p_R^2(t)dt$ and $\mathcal{E}_B(\tau) := \mathcal{E}\int_0^{T_s-\tau} p_R^2(t)dt$. The noise $\zeta(k;\tau)$ turns out to be the superposition of the following three terms:

$$\zeta_1(k;\tau) := \sqrt{\mathcal{E}} \sum_{m=0}^{1} s(2k-m-1) \int_0^{T_s} p_R(t+mT_s-\tilde{\tau}_0) \times \eta(t+2kT_s+\tau)dt$$

$$\zeta_2(k;\tau) := \sqrt{\mathcal{E}} \sum_{m=0}^{1} s(2k-m) \int_0^{T_s} p_R(t+mT_s-\tilde{\tau}_0) \times \eta\left(t+(2k-1)T_s+\tau\right) dt$$

$$\zeta_3(k;\tau) := \int_0^{T_s} \eta(t+2kT_s+\tau) \cdot \eta\left(t+(2k-1)T_s+\tau\right) dt.$$

Interestingly, these are similar to the noise terms one finds in TR or pilot-waveform-assisted modulation (PWAM), as well as in differential UWB systems [1], [5], [6], [20], [23]. To simplify the variance evaluation of $\zeta_1(k;\tau)$ and $\zeta_2(k;\tau)$, suppose that $\{s(k)\}$ are independent, identically distributed (i.i.d.) binary PAM symbols with zero mean and unit energy. With $\eta(t)$ in (3) being bandpass-filtered AWGN with zero mean and double-sided PSD $N_0/2$, we show in Appendix II that $\zeta_1(k;\tau)$, $\zeta_2(k;\tau)$, and $\zeta_3(k;\tau)$ can be approximated as

[1]Notice that any $\tau \in [\tau_0 - T_f + \tau_{0,L_0}, \tau_0 + c_0(0)T_c]$ can achieve equality in (6), so long as $\tau_{0,L_0} - T_f < c_0(0)T_c$. This may introduce a time uncertainty that is upper bounded by $\max\{T_f - \tau_{0,L_0}, c_0(0)T_c\} < T_f$. However, such a timing uncertainty does not affect BER, because it only induces a time shift to the channel estimate and does not give rise to ISI. It can also be easily resolved by invoking the TH code $c_u(0)$ of the desired user by performing a change detection test over the interval $[0, T_f]$.

mutually uncorrelated Gaussian variables with zero mean and correlation functions

$$\begin{aligned}\mathrm{E}\{\zeta_1(k;\tau)\zeta_1(l;\tau)\} &= \frac{\mathcal{E}_R N_0}{2}\delta_{k,l}\\ \mathrm{E}\{\zeta_2(k;\tau)\zeta_2(l;\tau)\} &= \frac{\mathcal{E}_R N_0}{2}\delta_{k,l}\\ \mathrm{E}\{\zeta_3(k;\tau)\zeta_3(l;\tau)\} &= \frac{N_0^2 BT_s}{2}\delta_{k,l}\end{aligned} \tag{11}$$

respectively, where $\delta_{k,l}$ denotes Kronecker's delta function. The overall noise $\zeta(k;\tau)$ in the symbol-rate samples $x(k;\tau)$ is also zero-mean Gaussian with correlation function

$$E\{\zeta(k;\tau)\zeta(l;\tau)\} = \left(\mathcal{E}_R N_0 + BT_s\frac{N_0^2}{2}\right)\delta_{k,l} =: \sigma_\zeta^2\delta_{k,l}.$$

*Remark 1:* As in TR and PWAM systems that rely on the cross correlation of two noisy received segments, our TDT samples also contain a "double-noise" term $\zeta_3(k;\tau)$. Its variance (derived in, e.g., [20]) is the product of two factors: one is the expected "squared-noise variance," namely, $N_0^2/2$; the other is the time-bandwidth product $BT_s$, where $B$ is the bandwidth of the receiver frontend and $T_s$ is the symbol duration. With UWB pulse duration $T_p$, we have $B \approx 1/T_p$, and thus $BT_s \approx T_s/T_p$, which is nothing but the spreading gain! As a result, this double-noise term is not worse for UWB than in any conventional CDMA system with the same spreading gain. Nevertheless, this double-noise term must be properly handled to avoid performance losses in TR and TDT systems. In the ensuing section, we will show how the effects of $\zeta(k;\tau)$ can be alleviated by averaging.

### A. Nondata-Aided (Blind) Mode

The mean square of the samples in (10) can be written as

$$\begin{aligned}&\mathrm{E}\left\{x^2(k;\tau)\right\}\\ &= \mathrm{E}\left\{\left[s(2k-2)\mathcal{E}_A(\tilde{\tau}_0)+s(2k)\mathcal{E}_B(\tilde{\tau}_0)\right]^2\right\}+\mathrm{E}\left\{\zeta^2(k;\tau)\right\}\\ &= \mathrm{E}\left\{\zeta^2(k;\tau)\right\} + \mathrm{E}\left\{s^2(2k-2)\mathcal{E}_A^2(\tilde{\tau}_0) + s^2(2k)\mathcal{E}_B^2(\tilde{\tau}_0)\right.\\ &\qquad \left. + 2s(2k-2)s(2k)\mathcal{E}_A(\tilde{\tau}_0)\mathcal{E}_B(\tilde{\tau}_0)\right\}\\ &= \mathcal{E}_A^2(\tilde{\tau}_0) + \mathcal{E}_B^2(\tilde{\tau}_0) + \sigma_\zeta^2\\ &= \frac{1}{2}\left[\mathcal{E}_A(\tilde{\tau}_0) + \mathcal{E}_B(\tilde{\tau}_0)\right]^2 + \frac{1}{2}\left[\mathcal{E}_A(\tilde{\tau}_0) - \mathcal{E}_B(\tilde{\tau}_0)\right]^2 + \sigma_\zeta^2.\end{aligned} \tag{12}$$

Now notice that $\mathcal{E}_A(\tilde{\tau}_0) + \mathcal{E}_B(\tilde{\tau}_0) = \mathcal{E}\int_0^{T_s} p_R^2(t)dt := \mathcal{E}_R$ is the constant energy of the unknown aggregate template at the receiver; and also that $\mathcal{E}_B(\tilde{\tau}_0) - \mathcal{E}_A(\tilde{\tau}_0)$ is uniquely maximized at $\tilde{\tau}_0 = 0$, since $\mathcal{E}_A(\tilde{\tau}_0)$ is minimized at $\tilde{\tau}_0 = 0$, and $\mathcal{E}_B(\tilde{\tau}_0)$ is maximized at $\tilde{\tau}_0 = 0$, by definition. Hence, $\mathrm{E}\{x^2(k;\tau)\}$ is maximized when $\tilde{\tau}_0 = 0$, or equivalently, $\tau = \tau_0$. Compactly written, the approach for *nondata-aided* TDT yields $\tau_0 = \arg\max_{\tau\in[0,T_s)} \mathrm{E}\{x^2(k;\tau)\}$.

As usual, the ensemble mean will be replaced in practice by its sample mean estimator obtained from $K$ pairs of symbol-long received segments $K^{-1}\sum_{k=1}^K x^2(k;\tau)$. We summarize the TDT algorithm in its NDA form as follows.

*Proposition 1:* Under **(as)**, unbiased and mean-square sense (mss)-consistent NDA (blind) TDT can be accomplished even when TH codes are present and the UWB multipath channel is unknown, using "dirty" $T_s$-long segments of the received waveform as follows:

$$\begin{aligned}\hat{\tau}_{0,\mathrm{nda}} &= \arg\max_{\tau\in[0,T_s)} y_{\mathrm{nda}}(K;\tau)\\ y_{\mathrm{nda}}(K;\tau) &:= \frac{1}{K}\sum_{k=1}^{K}\left(\int_{2kT_s}^{(2k+1)T_s} r(t+\tau)r(t+\tau-T_s)dt\right)^2.\end{aligned} \tag{13}$$

To show that $\hat{\tau}_{0,\mathrm{nda}}$ in (13) is mss-consistent, we start with the mean and variance of the *objective function* $y_{\mathrm{nda}}(K;\tau)$, which are given by (see Appendix III)

$$\begin{aligned}m_{\mathrm{nda}}(K;\tau) &:= \mathrm{E}\{y_{\mathrm{nda}}(K;\tau)\}\\ &= \frac{1}{2}\mathcal{E}_D^2(\tilde{\tau}_0) + \frac{\mathcal{E}_R^2}{2} + \sigma_\zeta^2\\ \sigma^2_{y_{\mathrm{nda}}}(K;\tau) &:= \mathrm{var}\{y_{\mathrm{nda}}(K;\tau)\}\\ &= \frac{2\sigma_\zeta^2}{K}\left[\mathcal{E}_R^2 + \mathcal{E}_D^2(\tilde{\tau}_0) + \sigma_\zeta^2\right]\\ &\quad + \frac{4}{K}\mathcal{E}_A^2(\tilde{\tau}_0)\mathcal{E}_B^2(\tilde{\tau}_0)\end{aligned} \tag{14}$$

where $\mathcal{E}_D^2(\tilde{\tau}_0) := [\mathcal{E}_A(\tilde{\tau}_0) - \mathcal{E}_B(\tilde{\tau}_0)]^2$. Notice that the basic idea behind our TDT estimator is that $\mathcal{E}_D^2(\tilde{\tau}_0)$ is maximized when $\tilde{\tau}_0 = 0$. Although terms $\mathcal{E}_R/2$ and $\sigma_\zeta^2$ are unknown because $p_R(t)$ is unknown, they remain constant $\forall\tau$ regardless of $p_R(t)$, and thus do not affect the peak-picking operation in finding $\hat{\tau}_0$. Additionally, the variance in (14) decays as $1/K$, establishing that $\hat{\tau}_{0,\mathrm{nda}}$ in (13) is mss-consistent.

### B. Data-Aided Mode

The number of samples $K$ required for reliable estimation can be reduced markedly if a *data-aided* approach is pursued [19]. Examining (12), we find that the constant term $[\mathcal{E}_A(\tilde{\tau}_0) + \mathcal{E}_B(\tilde{\tau}_0)]^2 = \mathcal{E}_R^2$ does not contain any information of $\tilde{\tau}_0$, and it is the energy-difference term $[\mathcal{E}_A(\tilde{\tau}_0) - \mathcal{E}_B(\tilde{\tau}_0)]^2$ that makes TDT operational. From (10), we further notice that $x(k;\tau)$ is guaranteed to contain the energy-difference term if the symbols $s(k)$ satisfy $s(2k-2) = -s(2k)$. These observations suggest that the training sequence $\{s(k)\}$ for DA TDT comprises a repeated pattern $(a, a, -a, -a)$ (or any of its circularly shifted versions) with $a$ being any $M$-ary PAM symbol; that is

$$s(k) = (-1)^{\lfloor \frac{k}{2}\rfloor}\cdot a. \tag{15}$$

This pattern is particularly attractive, because it simplifies (10) to

$$\begin{aligned}x(k;\tau) &= s(2k-1)\left[s(2k-2)\mathcal{E}_A(\tilde{\tau}_0) + s(2k)\mathcal{E}_B(\tilde{\tau}_0)\right] + \xi(k;\tau)\\ &= a^2\left[\mathcal{E}_A(\tilde{\tau}) - \mathcal{E}_B(\tilde{\tau})\right] + \xi(k;\tau)\end{aligned} \tag{16}$$

where we substituted $s(2k-1)=s(2k-2)=(-1)^{k-1}a$ and $s(2k)=(-1)^k a$. The noise term $\xi(k;\tau)$ in the DA mode is also the superposition of three terms

$$\xi_1(k;\tau):=\int_0^{T_s}\rho\left(t+(2k-1)T_s+\tau\right)\eta(t+2kT_s+\tau)dt$$

$$\xi_2(k;\tau):=\int_0^{T_s}\rho(t+2kT_s+\tau)\eta\left(t+(2k-1)T_s+\tau\right)dt$$

$$\xi_3(k;\tau):=\int_0^{T_s}\eta(t+2kT_s+\tau)\cdot\eta\left(t+(2k-1)T_s+\tau\right)dt$$

where the noise-free parts of the received segments are [c.f. (9) and (15)]

$$\begin{aligned}&\rho(t+2kT_s+\tau)\\&\quad=(-1)^{k-1}a\sqrt{\mathcal{E}}\left[p_R(t+T_s-\tilde{\tau}_0)-p_R(t-\tilde{\tau}_0)\right]\\&\rho\left(t+(2k-1)T_s+\tau\right)\\&\quad=(-1)^{k-1}a\sqrt{\mathcal{E}}\left[p_R(t+T_s-\tilde{\tau}_0)+p_R(t-\tilde{\tau}_0)\right]\end{aligned}\quad \forall t\in[0,T_s). \tag{17}$$

Using the fact that $\int_0^{T_s}\rho^2(t+2kT_s+\tau)dt=\int_0^{T_s}\rho^2(t+(2k-1)T_s+\tau)dt=a^2\mathcal{E}_R$, it can be readily proved (along the lines of Appendix II) that the variance of $\xi(k;\tau)$ is $\sigma_\xi^2=a^2\mathcal{E}_R N_0+N_0^2BT_s/2$.

Notice that in the DA mode, no expectation is taken with respect to $s(k)$, that is necessary in the blind approach in order to remove the unknown symbol effects (self-noise). As a result, we will show in the next section that $K^{-1}\sum_{k=1}^K x^2(k;\tau)$ converges faster to its expected value

$$\mathrm{E}\left\{x^2(k;\tau)\right\}=a^4\left[\mathcal{E}_A(\tilde{\tau})-\mathcal{E}_B(\tilde{\tau})\right]^2+\sigma_\xi^2. \tag{18}$$

A major benefit with DA TDT is very rapid acquisition, since, in principle, only $K=1$ pair of received symbol-long segments carrying as few as four training symbols, is sufficient at high signal-to-noise ratio (SNR). More specifically, with $K=1$, the single pair of "dirty templates" consists of

$$\begin{aligned}r(t+T_s+\tau)&=a\sqrt{\mathcal{E}}\left[p_R(t+T_s-\tilde{\tau}_0)+p_R(t-\tilde{\tau}_0)\right]\\&\quad+\eta(t+T_s+\tau)\\r(t+2T_s+\tau)&=a\sqrt{\mathcal{E}}\left[p_R(t+T_s-\tilde{\tau}_0)-p_R(t-\tilde{\tau}_0)\right]\\&\quad+\eta(t+2T_s+\tau)\end{aligned}$$

$\forall t\in[0,T_s)$, and their correlation yields

$$x(1;\tau)=a^2\left[\mathcal{E}_A(\tilde{\tau}_0)-\mathcal{E}_B(\tilde{\tau}_0)\right]+\xi(1;\tau)$$

which is guaranteed to contain the $[\mathcal{E}_A(\tilde{\tau}_0)-\mathcal{E}_B(\tilde{\tau}_0)]$ term that our TDT relies on. Of course, larger $K$ values will help average out the additive noise effects, and thus improve synchronization performance. Summarizing, our DA TDT approach is as follows.

*Proposition 2:* Under **(as)**, unbiased and mss-consistent DA TDT can also be accomplished, even when TH codes are present and the UWB multipath channel is unknown, using

$$\hat{\tau}_{0,\mathrm{da1}}=\arg\max_{\tau\in[0,T_s)}y_{\mathrm{da1}}(K;\tau)$$

$$y_{\mathrm{da1}}(K;\tau):=\frac{1}{K}\sum_{k=1}^K\left(\int_{2kT_s}^{(2k+1)T_s}r(t+\tau)r(t+\tau-T_s)dt\right)^2. \tag{19}$$

As with the blind mode, the DA mode requires only symbol-rate samples. Additionally, with the training pattern in (15), the DA mode enjoys rapid acquisition relying on a minimum of four training symbols, $[a,a,-a,-a]$.

The estimator (19) is essentially the same as (13), except that training symbols are employed in (19). These training symbols, however, are instrumental in improving the estimation performance. The mean and variance of $y_{\mathrm{da1}}(K;\tau)$ are readily found to be

$$\begin{aligned}&m_{\mathrm{da1}}(K;\tau):=\mathrm{E}\left\{y_{\mathrm{da1}}(K;\tau)\right\}=\mathcal{E}_D^2(\tilde{\tau}_0)+\sigma_\xi^2\\&\sigma^2_{y_{\mathrm{da1}}}(K;\tau):=\mathrm{var}\{y_{\mathrm{da1}}(K;\tau)\}=\frac{2\sigma_\xi^2}{K}\left[2\mathcal{E}_D^2(\tilde{\tau}_0)+\sigma_\xi^2\right].\end{aligned} \tag{20}$$

Again, as $K$ increases, $y_{\mathrm{da1}}(K;\tau)$ asymptotically converges to $\mathcal{E}_D^2(\tilde{\tau}_0)$, augmented uniformly by $\sigma_\xi^2\ \forall\tilde{\tau}$, and the estimate $\hat{\tau}_{0,\mathrm{da1}}$ relies merely on relative (as opposed to absolute) values of $\mathcal{E}_D^2(\tilde{\tau}_0)$ at different $\tilde{\tau}_0$'s. The estimator (19) is thus mss-consistent, as in the blind mode.

Comparing (20) with (14), we observe that $\sigma^2_{y_{\mathrm{da1}}}(K;\tau)<\sigma^2_{y_{\mathrm{nda}}}(K;\tau)\,\forall K,\tau$. This smaller variance leads to improved performance when estimating $\tau_0$ by peak-picking $y_{\mathrm{da1}}(K;\tau)$. In Section IV, we will further elaborate on performance differences under a coarse timing (acquisition) setting, and the comparison will corroborate our intuition.

*Proposition 2* reveals that the estimator we developed for blind timing applies to the DA mode without any modification, but with improved synchronization speed and accuracy. In fact, with our judiciously designed training pattern, further improvements are possible. First, notice that in the DA mode, we have from (16)

$$\mathrm{E}^2\left\{x(k;\tau)\right\}=a^4\left[\mathcal{E}_A(\tilde{\tau})-\mathcal{E}_B(\tilde{\tau})\right]^2. \tag{21}$$

That is, by taking the squared mean instead of the mean square, the noise variance term $\sigma_\xi^2$ in (18) vanishes. This observation leads us to the following result.

*Proposition 3:* Under **(as)** and with the training pattern in (15), unbiased and mss-consistent DA TDT can be accomplished using

$$\hat{\tau}_{0,\mathrm{da2}}=\arg\max_{\tau\in[0,T_s)}y_{\mathrm{da2}}(K;\tau)$$

$$y_{\mathrm{da2}}(K;\tau):=\left(\frac{1}{K}\sum_{k=1}^K\int_{2kT_s}^{(2k+1)T_s}r(t+\tau)r(t+\tau-T_s)dt\right)^2 \tag{22}$$

even with as few as four training symbols $[a,a,-a,-a]$.

The mean and variance of $y_{\rm da2}(K;\tau)$ can be easily obtained as

$$\begin{aligned} m_{\rm da2}(K;\tau) &:= \mathrm{E}\left\{y_{\rm da2}(K;\tau)\right\} \\ &= \mathcal{E}_D^2(\tilde{\tau}_0) + \frac{1}{K}\sigma_\xi^2 \\ \sigma^2_{y_{\rm da2}}(K;\tau) &:= \mathrm{var}\left\{y_{\rm da2}(K;\tau)\right\} \\ &= \frac{2\sigma_\xi^2}{K}\left[2\mathcal{E}_D^2(\tilde{\tau}_0) + \frac{\sigma_\xi^2}{K}\right]. \end{aligned} \tag{23}$$

Different from $y_{\rm da1}(K;\tau)$, $y_{\rm da2}(K;\tau)$ asymptotically converges to $\mathcal{E}_D^2(\tilde{\tau}_0)$. Moreover, its variance is further reduced by $2(K-1)\sigma_\xi^4/K^2$; that is, though the $\sigma_\xi^2$ term still decays as $1/K$, the $\sigma_\xi^4$ term decays as $1/K^2$. In the next section, we will show that this reduction in variance indeed improves the estimation of $\tau_0$.

*Remark 2:* Notice that both (19) and (22) rely on the same set of operations: correlation, averaging, and squaring. But the order of carrying out these operations is different. In (19), we have correlation followed by squaring and then averaging; whereas in (22), we have correlation followed by averaging and then squaring. Nevertheless, unlike (19), that is applicable to both blind and DA modes, the estimator (22) is valid only when our training pattern is employed.

Estimators (13), (19), and (22) all rely on averaging digital samples. If one opts to sacrifice complexity and average analog waveforms, then the estimation performance can be further improved in the DA mode. Specifically, further swapping the order of correlation and averaging, it follows from (17) that

$$\begin{aligned} &\mathrm{E}\left\{(-1)^{k-1} r\left(t+(2k-1)T_s+\tau\right)\right\} \\ &\quad = a\sqrt{\mathcal{E}}\left[p_R(t+T_s-\tilde{\tau}_0) + p_R(t-\tilde{\tau}_0)\right] \\ &\mathrm{E}\left\{(-1)^{k-1} r(t+2kT_s+\tau)\right\} \\ &\quad = a\sqrt{\mathcal{E}}\left[p_R(t+T_s-\tilde{\tau}_0) - p_R(t-\tilde{\tau}_0)\right]. \end{aligned} \tag{24}$$

Using these to form the correlation as in (5), we obtain

$$\int_0^{T_s} \mathrm{E}\left\{(-1)^k r\left(t+(2k+1)T_s+\tau\right)\right\} \times \mathrm{E}\left\{(-1)^k r(t+2kT_s+\tau)\right\} dt = a^2\left[\mathcal{E}_B(\tilde{\tau}_0) - \mathcal{E}_A(\tilde{\tau}_0)\right]$$

whose squared value is again $a^4[\mathcal{E}_A(\tilde{\tau}_0) - \mathcal{E}_B(\tilde{\tau}_0)]^2$, as in (21). We then have the following result.

*Proposition 4:* Under **(as)** and with the training pattern in (15), unbiased and mss-consistent DA TDT can be accomplished with as few as four training symbols using

$$\begin{aligned} \tilde{\tau}_{0,\rm da3} &= \arg\max_{\tau\in[0,T_s)} y_{\rm da3}(K;\tau) \\ y_{\rm da3}(K;\tau) &:= \left(\int_0^{T_s} \bar{r}(t+\tau)\bar{r}(t+\tau-T_s)dt\right)^2 \end{aligned} \tag{25}$$

where

$$\bar{r}(t) := \frac{1}{K}\sum_{k=1}^{K}(-1)^k r(t+2kT_s).$$

It is worth stressing that, as (19), the estimator (22) also relies on the training pattern (15).

To facilitate further analysis, let us write explicitly the averaged symbol-long received segments

$$\begin{aligned} \bar{r}(t+\tau) &= a\sqrt{\mathcal{E}}\left[p_R(t+T_s-\tilde{\tau}_0) - p_R(t-\tilde{\tau}_0)\right] + \bar{\eta}(t+\tau) \\ \bar{r}(t+\tau-T_s) &= a\sqrt{\mathcal{E}}\left[p_R(t+T_s-\tilde{\tau}_0) + p_R(t-\tilde{\tau}_0)\right] \\ &\quad + \bar{\eta}(t+\tau-T_s) \end{aligned}$$

where $\bar{\eta}(t) := K^{-1}\sum_{k=1}^{k}(-1)^k\eta(t+2kT_s)$. Notice that the PSD of the AGN term $\bar{\eta}(t)$ is $N_0/(2K)$, thanks to averaging. Letting $\bar{x}(\tau) := \int_0^{T_s}\bar{r}(t+\tau)\bar{r}(t+\tau-T_s)dt$, we have

$$\bar{x}(\tau) = a^2\left[\mathcal{E}_A(\tilde{\tau}_0) - \mathcal{E}_B(\tilde{\tau}_0)\right] + \bar{\xi}(\tau) \tag{26}$$

where $\bar{\xi}(\tau)$ is zero-mean Gaussian distributed with variance $\sigma_{\bar{\xi}}^2 = a^2\mathcal{E}_R N_0/K + N_0^2 BT_s/(2K^2)$. Notice that $\sigma_{\bar{\xi}}^2 < \sigma_\xi^2/K$ $\forall K > 1$. This is because while the variance of $\bar{\eta}(t)$ is reduced by $1/K$, that of the double-noise term is reduced by $1/K^2$.

*Remark 3:* Equation (26) reveals that the variance of the double-noise term can be reduced $1/K$ more than the single-noise term, as we mentioned in *Remark 1*. In fact, averaging the received segments before correlation can be interpreted as forming an estimate of the circularly shifted aggregate channel [17]. The resultant average estimate of the channel contains error, which comes merely from the additive noise. This error then gives rise to the double-noise term. If, on the other hand, one opts to estimate each and every multipath return and build a Rake receiver using these (or part of these) amplitude and delay estimates, then error will appear again. But with this option, the errors come not only from additive noise, but also from erroneous estimates of the delays [13]. Hence, the double-noise term is not particular to TDT synchronizers and TR-type receivers, but is always present when the channel is unknown. In addition, though the double-noise term in TDT affects timing-acquisition performance, it does not dictate alone the BER performance. This is because our TDT synchronizer can supply the required timing to any coherent demodulator, including Rake and TR.

Noticing that $y_{\rm da3}(K;\tau) = \bar{x}^2(\tau)$, the corresponding mean and variance are

$$\begin{aligned} m_{\rm da3}(K;\tau) &:= \mathrm{E}\left\{y_{\rm da3}(K;\tau)\right\} = \mathcal{E}_D^2(\tilde{\tau}_0) + \sigma_{\bar{\xi}}^2, \\ \sigma^2_{y_{\rm da3}}(K;\tau) &:= \mathrm{var}\left\{y_{\rm da3}(K;\tau)\right\} = 2\sigma_{\bar{\xi}}^2\left[2\mathcal{E}_D^2(\tilde{\tau}_0) + \sigma_{\bar{\xi}}^2\right]. \end{aligned} \tag{27}$$

Bearing the same form as (20), (27) is actually reminiscent of (23). Recalling the definition of $\sigma_{\bar{\xi}}^2$, and setting $a=1$, we have

$$\begin{aligned} \sigma_{\bar{\xi}}^2 &= \frac{1}{K}\mathcal{E}_R N_0 + \frac{1}{K^2}\frac{N_0^2 BT_s}{2} \le \frac{1}{K}\left(\mathcal{E}_R N_0 + \frac{N_0^2 BT_s}{2}\right) \\ &= \frac{\sigma_\xi^2}{K} = \frac{\sigma_\zeta^2}{K} \end{aligned}$$

where the inequality holds $\forall K > 1$. This implies that $y_{\rm da3}(K;\tau)$ has smaller variance and converges faster than $y_{\rm nda}(K;\tau)$, $y_{\rm da1}(K;\tau)$ or $y_{\rm da2}(K;\tau)$ $\forall K > 1$.

Standard deviations of $y(K;\tau)$s corresponding to *Propositions 1–4* are plotted in Fig. 2, with $\tau_0 = 0$, $K = 8$, and

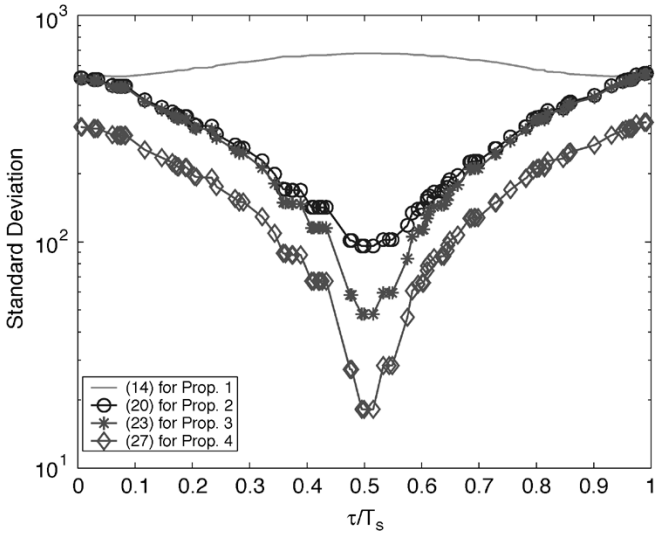


Fig. 2. Standard deviations of $y_{\rm nda}(K;\tau)$, $y_{\rm da1}(K;\tau)$, $y_{\rm da2}(K;\tau)$, and $y_{\rm da3}(K;\tau)$ for synchronizers in *Propositions 1–4*.

$\mathcal{E}/N_0 = 0$ dB. A multipath channel and a TH sequence are randomly generated and fixed for a set of randomly generated timing offsets. Parameters for these plots are detailed in Section VI. Fig. 2 confirms that $y_{\rm da3}(K;\tau)$ yields the smallest variance $\forall\tau$. Performance comparison in Section IV and further simulations in Section VI will corroborate that indeed the TDT synchronizer of *Proposition 4* yields the best synchronization performance.

Summarizing, in a point-to-point link, we derived four $\hat{\tau}_0$ estimators in *Propositions 1–4*. The ones in *Propositions 1* and *2* are essentially identical; that is, (13) is an estimator applicable to both DA and NDA settings. *Proposition 2* indicates that our training pattern (15) enables faster synchronization with higher accuracy. Based on our training pattern, the estimator (22) improves performance using the same discrete-time samples taken at symbol rate. As always, a performance-complexity tradeoff emerges here. Though (25) gives the best performance by reducing the double-noise term variance, it requires analog delay lines to average dirty templates. More important, we will prove in Section V that estimators (22) and (25) remain operational, even when multiple (asynchronous) users are present.

The $\hat{\tau}_0$ estimators in *Propositions 1–4* allow for timing acquisition at any desirable resolution, constrained only by the affordable complexity: 1) coarse timing with low complexity, e.g., by picking the maximum over $N_f$ candidate offsets $\tau = nT_f$, where integer $n \in [0, N_f)$; 2) fine timing with higher complexity at the chip resolution with $\tau = iT_c$, $i \in [0, N_c)$; and 3) adaptive timing estimation (tracking) with voltage-controlled clock (VCC) circuits.

## IV. Performance Comparisons

In the preceding section, we introduced four $\hat{\tau}_0$ estimators (each with distinct merits) along with the mean and variance of their objective functions $y(K;\tau)$. Here we compare their performance in a coarse timing (acquisition) setup, where the $N_i$ candidate offsets are $\tau = nT_i$ with integer $n \in [0, N_i - 1]$ and $T_i := T_s/N_i$. For any $n \in [0, N_i - 1]$, the objective function $y(K;\tau)$ has mean and variance as in (14), (20), (23), or (27). Now instead of estimating the true $\tau_0$, coarse timing aims at finding $n^*$ such that $|n^*T_i - \tau_0| < T_i$; that is, *detecting* $n^*$ such that $m(K;n^*T_i) = \max_n\{m(K;nT_i)\}$. The unifying detector encompassing *Propositions 1–4* is

$$\hat{n}^* = \arg\max_n y(K;nT_i).$$

The probability of detection is then given by

$$P_d(n^*) = \Pr\{\hat{n}^* = n^*\} = \Pr\left\{y(K;n^*T_i) = \max_n y(K;nT_i)\right\}.$$

Notice that at any given SNR, regardless of $p_R(t)$ and $K$, $P_d(n^*)$ generally depends on $n^*$. This is because the noise terms of $y(K;nT_i)$ are correlated across $n$ since the observation windows are overlapping. For analytical tractability, we will assume independence[2] of $y(K;nT_i)$ across $n$. Denoting the probability density function (pdf) of $y(K;nT_i)$ as $f_{K,n}(y)$, the probability of detection can be explicitly written as

$$P_d = \int_{-\infty}^{+\infty} f_{K,n^*}(y_0) \prod_{n\neq n^*} \left( \int_{-\infty}^{y_0} f_{K,n}(y_1)dy_1 \right) dy_0. \quad (28)$$

This expression involves $N_i$-fold integration, which is not only cumbersome to evaluate, but also numerically nonrobust, especially when $N_i$ exceeds 100. To compare $P_d$ associated with various TDT estimators, we resort to its lower bounds that often bear much simpler forms than (28). A widely adopted lower bound is the union bound (see, e.g., [12, Ch. 5])

$$P_d \geq 1 - \sum_{n\neq n^*} \int_{-\infty}^{\infty} f_{K,n^*}(y_0) \int_{y_0}^{\infty} f_{K,n}(y_1)dy_1\, dy_0 \quad (29)$$

which is the complement of the *sum* of the pairwise probabilities of miss. However, it is well known that the union bound is very loose, and can, at times, be negative at low SNR. Instead, using Bayes' rule, we can derive a lower bound similar to [9] which is much tighter than the union bound, especially at low SNR, and is expressed as the *product* of the pairwise probabilities of detection

$$P_d \geq \underline{P}_d := \prod_{n\neq n^*} \int_{-\infty}^{+\infty} f_{K,n^*}(y_0) \int_{-\infty}^{y_0} f_{K,n}(y_1)dy_1 dy_0. \quad (30)$$

Arguing through the central limit theorem, we can consider that $y(K;nT_i)$'s are Gaussian distributed, in which case the lower bound in (30) becomes

$$\underline{P}_d = \prod_{n\neq n^*} Q\left( \frac{m(K;n^*T_i) - m(K;nT_i)}{\sqrt{\sigma_y^2(K;n^*T_i) + \sigma_y^2(K;nT_i)}} \right) \quad (31)$$

where $Q(\cdot)$ is the complementary cumulative distribution function (cdf) of a Gaussian distribution with zero mean and unit

[2]Although this assumption is idealistic, our simulations will illustrate that the analytical comparison under this assumption serves as a lower bound on the simulated probability of detection.

variance. According to (14), (20), (23), and (27), and for any given $n$, $n^*$, and $K > 1$, we then have

$$\begin{aligned} & m_{\rm nda}(K;n^*T_i) - m_{\rm nda}(K;nT_i) \\ &= m_{\rm da1}(K;n^*T_i) - m_{\rm da1}(K;nT_i) \\ &= m_{\rm da2}(K;n^*T_i) - m_{\rm da2}(K;nT_i) \\ &= m_{\rm da3}(K;n^*T_i) - m_{\rm da3}(K;nT_i) \end{aligned}$$

and

$$\begin{aligned} & \sigma^2_{y_{\rm nda}}(K;n^*T_i) + \sigma^2_{y_{\rm nda}}(K;nT_i) \\ &> \sigma^2_{y_{\rm da1}}(K;n^*T_i) + \sigma^2_{y_{\rm da1}}(K;nT_i) \\ &> \sigma^2_{y_{\rm da2}}(K;n^*T_i) + \sigma^2_{y_{\rm da2}}(K;nT_i) \\ &> \sigma^2_{y_{\rm da3}}(K;n^*T_i) + \sigma^2_{y_{\rm da3}}(K;nT_i) \end{aligned} \quad (32)$$

for the estimators corresponding to *Propositions 1–4*. Equations (31) and (32) reveal that

$$\underline{P}_{d,\rm nda} < \underline{P}_{d,\rm da1} < \underline{P}_{d,\rm da2} < \underline{P}_{d,\rm da3} \quad \forall K > 1.$$

As expected, DA TDT outperforms blind TDT. Even with the same training pattern, performance can be improved at the price of higher complexity. Although the performance comparisons carried out in this section consider a timing-acquisition setting, the essential conclusions hold even for fine timing which corresponds to $T_i \to 0$.

Of course, our analysis here in terms of a lower bound on the probability of detection relies on the independent Gaussian assumption and can only provide qualitative comparisons among our TDT estimators. Exact variance analysis of the timing estimators is out of the scope of this paper, whose emphasis is on the TDT concept and algorithms, but constitutes certainly an important direction for our future work.

## V. Multiuser TDT

The timing algorithms we developed in Section III are for a point-to-point link where MUI is treated as noise. This is reasonable in a multiuser setting, provided that user separability is ensured through channelization. But even in such cases, user separation with despreading relies heavily on timing. To explore DA TDT in a multiuser setup, suppose we wish to synchronize to a single desired user (say, user 0) who is transmitting the training pattern $(a, a, -a, -a)$ and is received in the presence of other asynchronous users communicating information-bearing i.i.d. symbols. Equation (10) now becomes

$$x(k;\tau) = \sum_{u=0}^{N_u-1} x_u(k;\tau) = \sum_{u=0}^{N_u-1} s_u(2k-1)\left[s_u(2k)\mathcal{E}_{u,B}(\tilde{\tau}_u) + s_u(2k-2)\mathcal{E}_{u,A}(\tilde{\tau}_u)\right] + \xi(k;\tau) \quad (33)$$

where $\mathcal{E}_{u,A}(\tilde{\tau}_u) := \mathcal{E}_u \int_{T_s-\tilde{\tau}_u}^{T_s} p^2_{u,R}(t)dt$, $\mathcal{E}_{u,B}(\tilde{\tau}_u) := \mathcal{E}_u \int_0^{T_s-\tilde{\tau}_u} p^2_{u,R}(t)dt$ and $\tilde{\tau}_u := [\tau_u - \tau]_{T_s}$ are as defined before, but with symbols, channels, and offsets being user-dependent; thus allowing for both downlink and uplink operations. With binary PAM symbols and $a = 1$, the noise variance turns out to be $\sigma^2_\xi = \sum_{u=0}^{N_u-1} \mathcal{E}_{u,R} N_0 + N_0^2 B T_s/2$. As we argued in Section III, the noise-free part of the desired user's samples at the dirty-template correlator output obey [c.f. (16)]

$$\chi_0(k;\tau) = \mathcal{E}_{0,A}(\tilde{\tau}_0) - \mathcal{E}_{0,B}(\tilde{\tau}_0).$$

Substituting the latter into (33), we obtain

$$x(k;\tau) = \chi_0(k;\tau) + \sum_{u\neq 0} s_u(2k-1)\left[s_u(2k-2)\mathcal{E}_{u,A}(\tilde{\tau}_u) + s_u(2k)\mathcal{E}_{u,B}(\tilde{\tau}_u)\right] + \xi(k;\tau)$$

where $s_u(k)$'s are zero-mean i.i.d. information symbols transmitted by the $u(\neq 0)$th user.

If we now average (without squaring), as described in *Proposition* 3, we obtain $\mathrm{E}\{x(k;\tau)\} = \mathrm{E}\{x_0(k;\tau)\} = \mathcal{E}_{0,B}(\tilde{\tau}_0) - \mathcal{E}_{0,A}(\tilde{\tau}_0)$ simply because $\mathrm{E}\{\chi_u(k;\tau)\} = 0$. This observation suggests that the single-user TDT estimator we summarized in *Proposition 3* is operational even in a multiuser environment. In fact, so is the one in *Proposition 4*, as we will prove next.

The "dirty templates" in such a setting bear the form

$$r(t+kT_s+\tau) = \sum_{u=0}^{N_u-1} \rho_u(t+kT_s+\tau) + \eta(t+kT_s+\tau) \quad \forall t \in [0, T_s)$$

where $\rho_u(t+kT_s+\tau)$ is given by (17), if $u = 0$; and by (9), otherwise. Evidently, (9) has zero mean with i.i.d. zero-mean symbols; whereas the mean values of (17) are given in (24). As a result, we have

$$\begin{aligned} & \mathrm{E}\left\{(-1)^{\lfloor \frac{k}{2} \rfloor} r(t+kT_s+\tau)\right\} \\ &= \mathrm{E}\left\{(-1)^{\lfloor \frac{k}{2} \rfloor} r_0(t+kT_s+\tau)\right\} \\ &= \sqrt{\mathcal{E}}\left[p_{0,R}(t+T_s-\tilde{\tau}_0) + (-1)^k p_{0,R}(t-\tilde{\tau}_0)\right] \end{aligned}$$

which indicates that the single-user TDT estimator we summarized in *Proposition 4* can also be applied in a multiuser environment. Summarizing, we have established the following.

*Proposition 5:* Under **(as)** and with the desired user transmitting the training pattern in (15) and other users transmitting zero-mean i.i.d. information symbols, mss-consistent DA TDT can be accomplished with as few as four training symbols using either (19) or (22), without requiring any knowledge on these users' channels or timing information.

*Remark 4:* Our TDT-based timing algorithms in *Propositions 1–5* are well motivated when the dense multipath channel is unknown, and a noise-free and offset-free "clean" template of the distorted waveform is not available. But even over AWGN channels where the clean template is simply $p(t)$, our TDT-based algorithms still have clear advantages over conventional ones. In this case, the received waveform consists of episodic signals. With conventional synchronizers using the clean $p(t)$ template, symbol-level (coarse) synchronization is impossible, because the frame-by-frame sliding correlation will mostly capture noise only. Hence, sliding correlation lags have to be computed every $T_p$ seconds over a symbol duration of $T_s \approx N_f N_c T_p$, which translates to searching for the maximum over $N_f N_c$ lags. On the other hand, our TDT-based algorithms rely on the correlation between two dirty templates subject to the same frame-level shift, and are guaranteed to capture the signal energy even in the coarse timing stage. As a result, one can conduct symbol-level synchronization in $N_f$ steps (one per frame), and follow it up with frame-level (fine) synchronization in $N_c$ steps (one per $T_p$).

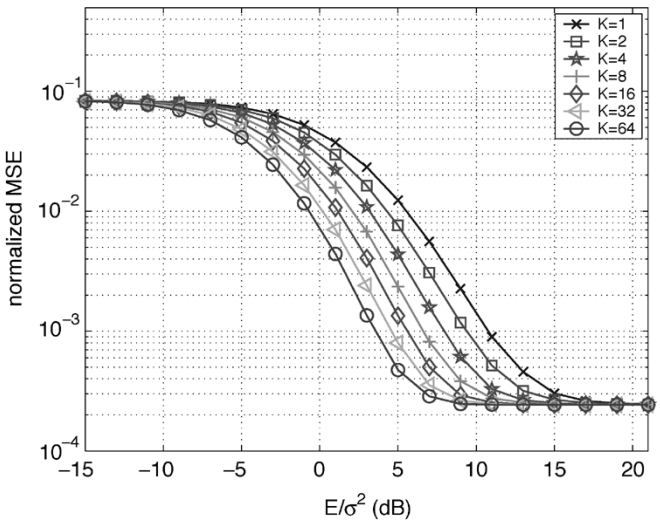


Fig. 3. Normalized MSE for the DA TDT synchronizer of *Proposition 2* with various $K$ values, in a single-user link.

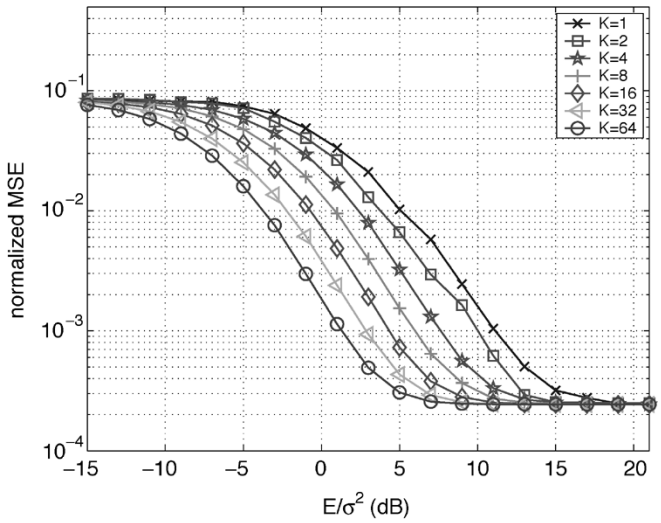


Fig. 4. Normalized MSE for the DA TDT synchronizer of *Proposition 3* with various $K$ values, in a single-user link.

In UWB systems having typically very large $N_f$ and $N_c$ values, the complexity reduction is considerable.

It is also worth mentioning that though our timing algorithms for point-to-point links and in the presence of multiple users are derived for fast TH or short DS spreading codes, the DA TDT algorithms in *Propositions 2–5* can be easily generalized to account for slow TH and DS codes with multisymbol period, by alternately transmitting $a$'s and $-a$'s every two periods of the TH/DS sequence.

## VI. Simulations

In this section, we perform simulations to test the performance of our TDT algorithms. The UWB pulse is the second derivative of the Gaussian function with unit energy and duration $T_p \approx 1$ ns. The multipath channels are generated using the channel model in [3], with real channel taps and parameters $(1/\Lambda, 1/\lambda, \Gamma, \gamma) = (43, 0.4, 7.1, 4.3)$ ns. The frame duration is chosen to be $T_f = 35$ ns. Each symbol duration contains $N_f = 32$ frames. The performance of our timing algorithms is tested for various values of $K$. And $\epsilon$ is randomly generated from a uniform distribution over $[0, T_s)$. We used a random TH code uniformly distributed over $[0, N_c - 1]$, with $N_c = 35$, and $T_c = 1.0$ ns. In all simulations, only frame-level coarse timing is performed; i.e., $N_i = N_f$.

We first test the mean square error (MSE) of our DA TDT algorithms summarized in *Propositions 2–4* over a single-user link. The MSE is normalized with respect to $T_s^2$, and plotted versus $\mathcal{E}/N_0$ in Figs. 3–5. With $K = 1$, these estimators based on our training pattern yield almost identical performance. But as $K$ increases, not only the normalized MSE decreases monotonically for all synchronizers, but also the difference among them becomes more noticeable. Increasing SNR also helps to reduce the normalized MSE. At medium SNR, all curves reach an error floor, which is reasonable, since only coarse timing with $T_f$ resolution is performed. This error floor can be mitigated by fine timing (tracking), which is beyond the scope of this paper.

Next, in Fig. 6, we plot with solid curves the normalized MSE of the blind TDT algorithm in *Proposition 1*. Different from the

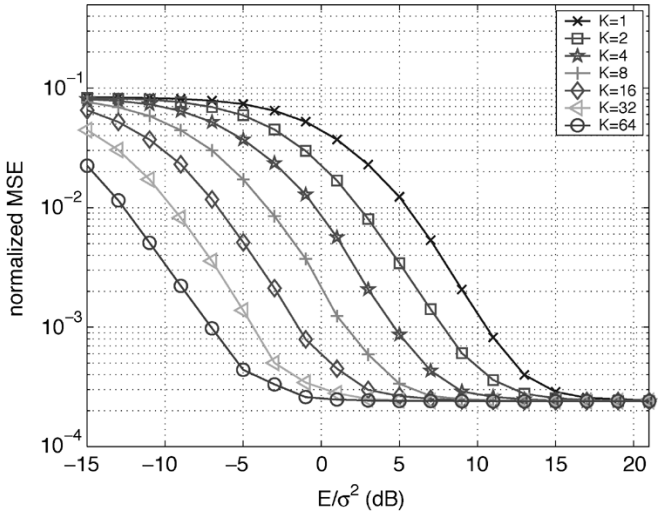


Fig. 5. Normalized MSE for the DA TDT synchronizer of *Proposition 4* with various $K$ values, in a single-user link.

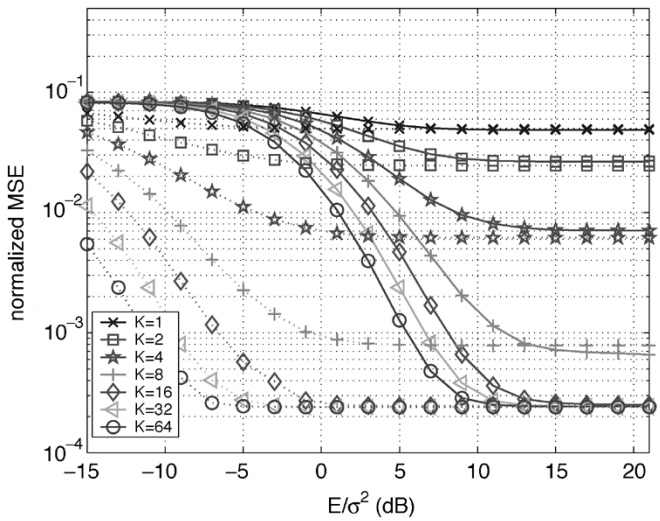


Fig. 6. Solid curves: Normalized MSE for the NDA TDT synchronizer of *Proposition 1*. Dotted curves: Normalized MSE for the "idealized" NDA TDT synchronizer.

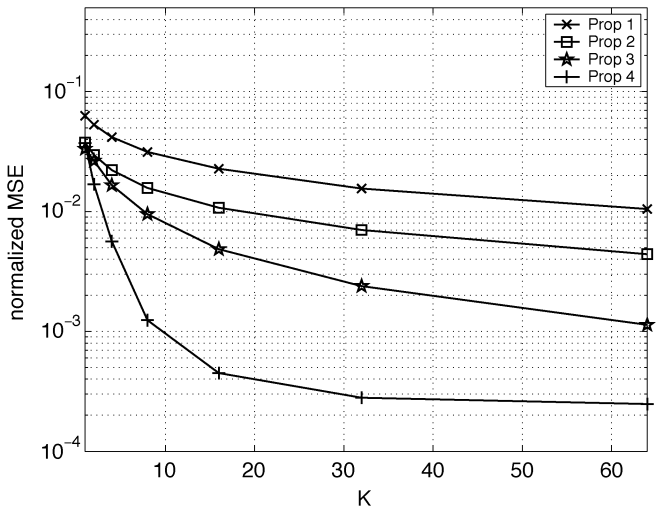


Fig. 7. Normalized MSE of $\hat{\tau}_0$ versus $K$ with $\mathcal{E}/N_0 = 1$ dB, in a single-user link.

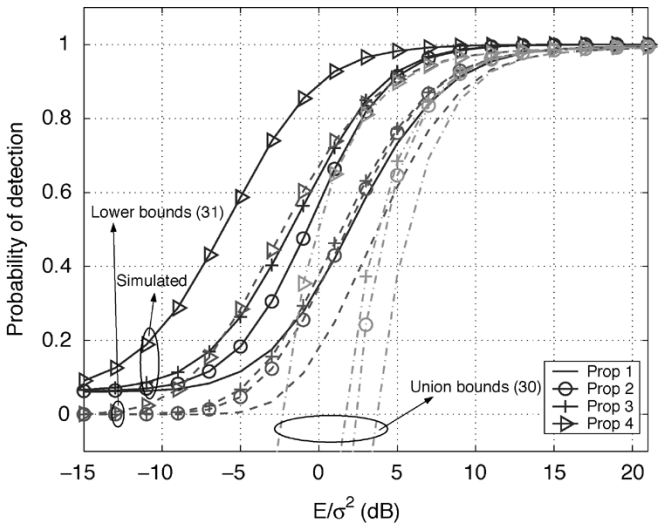


Fig. 8. Probability of detection and lower bounds versus SNR with $K = 8$, in a single-user link.

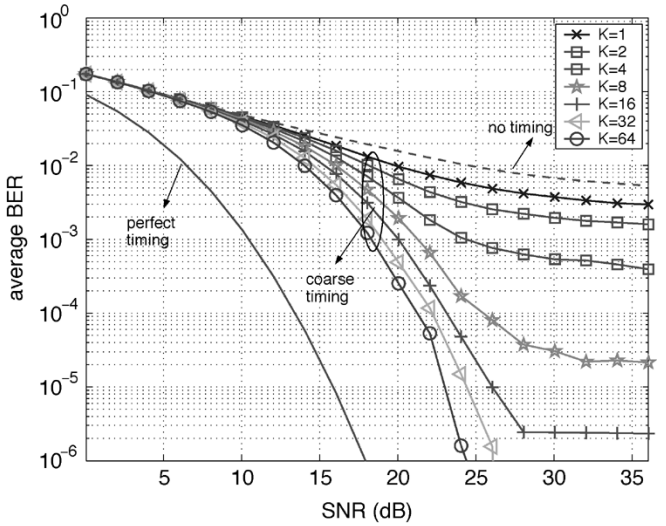


Fig. 9. Average BER for the NDA TDT synchronizer of *Proposition 1* with various $K$ values, in a single-user link.

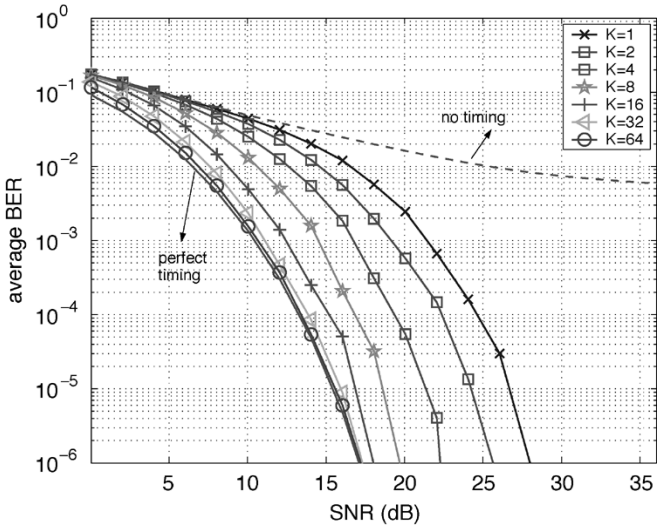


Fig. 10. Average BER for the DA TDT synchronizer of *Proposition 4* with various $K$ values, in a single-user link.

DA ones which share the same level of error floor, the blind algorithm exhibits higher error floors with smaller $K$ values. This is caused by insufficient averaging among random information symbols, which is not the case with the aid of the training pattern. For benchmarking purposes, we also plot (with dotted curves) the normalized MSE of an "idealized" blind timing algorithm, which assumes that a perfectly "clean" copy of the circularly shifted aggregate channel is available so that the double-noise term vanishes. In this case, $K$ refers to the number of correlations instead of pairs of dirty templates. Interestingly, such an "ideal" operation yields better performance only at low SNR, and converges to the blind TDT curves after 10 dB.

To further compare our synchronizers given in *Propositions 1–4*, we plot their normalized MSE versus $K$ at $\mathcal{E}/N_0 = 1$ dB, as shown in Fig. 7. These curves are consistent with our analyses in Section III. In Fig. 8, the simulated probability of detection versus SNR, together with its analytical lower bound in (31), are shown with $K = 8$ for our TDT synchronizers in *Propositions 1–4*. As expected, the lower bounds are rather pessimistic, but these curves correctly predict the relative performance of these synchronizers. The union bounds in (29) are also shown in Fig. 8. They are too loose to give meaningful indications at low-to-medium SNR.

Translating the synchronization performance into BER performance while isolating mistiming from channel-estimation errors, we suppose that channel estimation takes place after timing acquisition, and the channel estimate is error-free. Figs. 9 and 10 depict BER corresponding to the TDT synchronizers of *Propositions 1* and *4*, together with perfect timing and no timing, for various $K$ values. Again, as $K$ increases, BER decreases monotonically. Notice that even with $K = 1$, considerable improvement in BER performance is observed. In particular, DA TDT with $K = 32$ and $K = 64$ yields BER curves almost identical to the one corresponding to perfect timing. Once again, the gap can be further reduced by fine timing/tracking.

In Fig. 11, the normalized MSE corresponding to (22) in the presence of two interfering users is plotted. The two interfering users are asynchronous relative to the desired user, and are transmitting information symbols with 6 and 10 dB less SNR than the

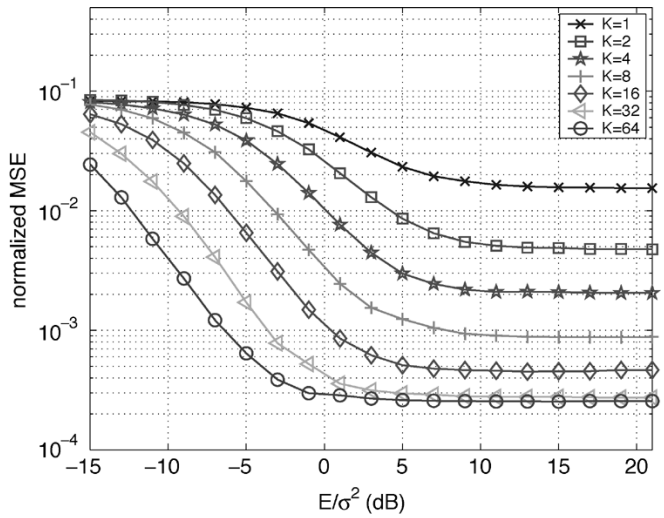


Fig. 11. Normalized MSE for the DA TDT synchronizer of *Proposition 4* with various $K$ values, in a multiuser environment.

desired one. Although the training pattern and synchronizer are the same as used for Fig. 5, the multiuser case exhibits worse performance as well as $K$-dependent error floors. These are induced by the MUI, since no MUI suppression is invoked in this example.

## VII. Conclusions

In this paper, we established a novel criterion for UWB timing synchronization, that we termed TDT. For a point-to-point link, we developed low-complexity TDT algorithms with and without training symbols, and compared their performance by analysis and simulations. In addition, we designed a simple training pattern which not only provides speedup for timing a single user, but also enables timing a desired user in a multiuser setup. Relying on simple integrate-and-dump operations such as TR, our TDT algorithms provide timing information that is needed by TR without incurring TR's severe loss in spectral efficiency. Our TDT algorithms can also be applied to narrowband systems, provided that ISI is absent. In our future research agenda, we plan to carry out asymptotic variance analysis in single- and multiuser environments, develop tracking-loop-based adaptive algorithms for fine timing, as well as investigate synchronization with pulse position modulation and in the presence of ISI. Additionally, the analog TDT algorithms we presented here require analog delay lines that can be challenging in UWB systems. It would be interesting to investigate digital implementations of these algorithms (e.g., using sigma-delta quantizers) and compare them with their analog counterparts.

## Appendix I
## Proof of Equation (8)

For any given $k$, $\tau$, and $\tau_0$, the index $n$ contributes a nonzero summand in (7) if the argument of $p_R(\cdot)$ stays within the range $[0, T_s)$; that is $0 \le t + kT_s + \tau - nT_s - \tau_0 < T_s$. Upon defining $k_{\tau_0} := \lfloor (\tau_0 - \tau)/T_s \rfloor$ and $\tilde{\tau}_0 := [\tau_0 - \tau]_{T_s}$, and rearranging terms in the inequality, we obtain $-t + \tilde{\tau}_0 \le (k - n - k_{\tau_0})T_s < T_s - t + \tilde{\tau}_0$. For $t \in [0, T_s)$, it follows that $-T_s + \tilde{\tau}_0 < (k - n - k_{\tau_0})T_s < T_s + \tilde{\tau}_0$, or equivalently, $-1 + (\tilde{\tau}_0/T_s) < k - n - k_{\tau_0} < 1 + (\tilde{\tau}_0/T_s)$. By definition, $k_{\tau_0}$ is an integer, and $\tilde{\tau}_0/T_s \in [0, 1)$. As a result, we have $0 \le k - n - k_{\tau_0} \le 1$. There are thus only two $n$ values that contribute nonzero summands in (7), and these $m$ values are $n = k - k_{\tau_0}$ and $n = k - k_{\tau_0} - 1$.

## Appendix II
## Proof of Equation (11)

We will derive in detail the autocorrelation function of the sampled noise $\zeta_1(k;\tau)$. That of $\zeta_2(k;\tau)$ can be obtained similarly. The reader is referred to [20, Appendix I] for detailed derivation of the autocorrelation function for the double-noise term $\zeta_3(k;\tau)$.

By definition, the autocorrelation funcption of $\zeta_1(k;\tau)$ is given by

$$\begin{aligned}
&\mathrm{E}\{\zeta_1(k;\tau)\zeta_1(l;\tau)\} \\
&\quad = \mathcal{E}\cdot \mathrm{E}\left\{\left(\sum_{m=0}^{1} s(2k-m-1) \right.\right. \\
&\qquad \left. \times \int_0^{T_s} p_R(t+mT_s-\tilde{\tau}_0)\eta(t+2kT_s+\tau)dt\right) \\
&\qquad \times \left(\sum_{m=0}^{1} s(2l-m-1) \right. \\
&\qquad \left.\left. \times \int_0^{T_s} p_R(t+mT_s-\tilde{\tau}_0)\eta(t+2lT_s+\tau)dt\right)\right\} \\
&\quad = \mathcal{E}\cdot \mathrm{E}\left\{\left(\sum_{m=0}^{1} s(2k-m-1) \right.\right. \\
&\qquad \left.\left. \times \int_0^{T_s} p_R(t+mT_s-\tilde{\tau}_0)\eta(t+2kT_s+\tau)dt\right)^2\right\} \\
&\qquad \times \delta_{k,l}
\end{aligned}$$

where in establishing the second equality, we used $\mathrm{E}\{s(k)s(l)\} = 0\ \forall K \ne l$. Consequently, we obtain

$$\begin{aligned}
&\mathrm{E}\{\zeta_1(k;\tau)\zeta_1(l;\tau)\} \\
&\quad = \mathcal{E}\sum_{m=0}^{1}\int_0^{T_s}\int_0^{T_s} p_R(t_1+mT_s-\tilde{\tau}_0)p_R(t_2+mT_s-\tilde{\tau}_0) \\
&\qquad \times \mathrm{E}\{\eta(t_1+2kT_s+\tau)\eta(t_2+2kT_s+\tau)\}\,dt_1dt_2\,\delta_{k,l}.
\end{aligned}$$

Using [20, Eqs. (37)–(38)], the following result can be obtained:

$$\begin{aligned}
&\mathrm{E}\{\zeta_1(k;\tau)\zeta_1(l;\tau)\} \\
&\quad \approx \frac{\mathcal{E}N_0}{2}\left(\int_0^{T_s} p_R^2(t+T_s-\tilde{\tau}_0)dt + \int_0^{T_s} p_R^2(t-\tilde{\tau}_0)dt\right)\delta_{k,l} \\
&\quad = \frac{\mathcal{E}_R N_0}{2}\delta_{k,l}.
\end{aligned}$$

## Appendix III
## Proof of Equation (14)

The expected value of $y_{\mathrm{nda}}(K;\tau)$ in (13) can be easily obtained as [c.f. (12)]

$$m_{\mathrm{nda}}(K;\tau) = \frac{1}{K}\sum_{k=1}^{K}\mathrm{E}\{x^2(k;\tau)\} = \mathcal{E}_A^2 + \mathcal{E}_B^2 + \sigma_\zeta^2.$$

To obtain its variance, first notice that by definition

$$\mathrm{var}\left\{\frac{1}{K}\sum_{k=1}^{K}x^2(k;\tau)\right\}=\mathrm{E}\left\{\left(\frac{1}{K}\sum_{k=1}^{K}x^2(k;\tau)\right)^2\right\}-\mathrm{E}^2\left\{\frac{1}{K}\sum_{k=1}^{K}x^2(k;\tau)\right\}$$

where $\mathrm{E}\{((1/K)\sum_{k=1}^{K}x^2(k;\tau))^2\}=(1/K^2)\sum_{k=1}^{K}\sum_{l=1}^{K}\mathrm{E}\{x^2(k;\tau)x^2(l;\tau)\}$. Depending on $K$ and $l$ values, and with binary PAM, $\mathrm{E}\{x^2(k;\tau)x^2(l;\tau)\}$ can be computed by considering two cases

$$\mathrm{E}\left\{x^2(k;\tau)x^2(l;\tau)\right\}=\begin{cases}\left(\mathcal{E}_A^2+\mathcal{E}_B^2+\sigma_\zeta^2\right)^2+\sigma_\zeta^4+4\sigma_\zeta^2\left(\mathcal{E}_A^2+\mathcal{E}_B^2\right)+4\mathcal{E}_A^2\mathcal{E}_B^2, & \text{if } k=l\\ \left(\mathcal{E}_A^2+\mathcal{E}_B^2+\sigma_\zeta^2\right)^2, & \text{else.}\end{cases}$$

Adding them up with appropriate weights, we obtain

$$\sigma^2_{y_{\mathrm{nda}}}(K;\tau)=\frac{2\sigma_\zeta^2}{K}\left[\mathcal{E}_R^2+(\mathcal{E}_A-\mathcal{E}_B)^2+\sigma_\zeta^2\right]+\frac{4}{K}\mathcal{E}_A^2\mathcal{E}_B^2.$$

## REFERENCES


[1] J. D. Choi and W. E. Stark, "Performance of ultra-wideband communications with suboptimal receivers in multipath channels," *IEEE J. Sel. Areas Commun.*, vol. 20, no. 9, pp. 1754–1766, Dec. 2002.

[2] R. Fleming, C. Kushner, G. Roberts, and U. Nandiwada, "Rapid acquisition for ultra-wideband localizers," in *Proc. Conf. Ultra-Wideband Syst. Technol.*, Baltimore, MD, May 20–23, 2002, pp. 245–250.

[3] J. R. Foerster, "Channel Modeling Sub-Committee Report Final,", IEEE P802.15-02/368r5-SG3a, IEEE P802.15 Working Group for WPAN, Nov. 2002.

[4] J. R. Foerster, E. Green, S. Somayazulu, and D. Leeper. (2001) Ultra-wideband technology for short or medium range wireless communications. *Intel Technol. J. Q2* [Online]. Available: http://developer.intel.com/technology/itj

[5] M. Ho, V. Somayazulu, J. Foerster, and S. Roy, "A differential detector for an ultra-wideband communications system," in *Proc. Veh. Technol. Conf.*, Birmingham, AL, May 4–9, 2002, pp. 1896–1900.

[6] R. T. Hoctor and H. W. Tomlinson, "Delay-hopped transmitted-reference RF communications," in *Proc. Conf. Ultra-Wideband Syst. Technol.*, Baltimore, MD, May 20–23, 2002, pp. 265–269.

[7] ——, "An overview of delay-hopped, transmitted-reference RF communications," *G.E. Res. Dev. Center, Tech. Inf. Ser.*, pp. 1–29, Jan. 2002.

[8] E. A. Homier and R. A. Scholtz, "Rapid acquisition of ultra-wideband signals in the dense multipath channel," in *Proc. Conf. Ultra-Wideband Syst. Technol.*, Baltimore, MD, May 20–23, 2002, pp. 105–110.

[9] L. W. Hughes, "A simple upper bound on the error probability for orthogonal signals in white noise," *IEEE Trans. Commun.*, vol. 40, no. 4, p. 670, Apr. 1992.

[10] J. Y. Lee and R. A. Scholtz, "Ranging in a dense multipath environment using an UWB radio link," *IEEE J. Sel. Areas Commun.*, vol. 20, no. 9, pp. 1677–1683, Dec. 2002.

[11] D. Porrat and D. Tse, "Bandwidth scaling in ultra wideband communications," in *Proc. 41st Allerton Conf.*, Monticello, IL, Oct. 1–3, 2003, [CD-ROM].

[12] J. Proakis, *Digital Communications*, 4th ed. New York: McGraw-Hill, 2001.

[13] H. Sheng, R. You, and A. M. Haimovich, "Performance analysis of ultra-wideband Rake receivers with channel delay estimation errors," in *Proc. Conf. Inf. Sci. Syst.*, Princeton, NJ, Mar. 17–19, 2004, pp. 921–926.

[14] Z. Tian and G. B. Giannakis, "BER sensitivity to mistiming in ultra-wideband communications—Part I: Nonrandom channels," *IEEE Trans. Signal Process.*, vol. 53, no. 4, pp. 1550–1560, Apr. 2005.

[15] ——, "Data-aided ML timing acquisition in ultra-wideband radios," in *Proc. Conf. Ultra-Wideband Syst. Technol.*, Reston, VA, Nov. 16–19, 2003, pp. 142–146.

[16] Z. Wang and G. B. Giannakis, "Wireless multicarrier communications: Where Fourier meets Shannon," *IEEE Signal Process. Mag.*, vol. 17, no. 3, pp. 29–48, May 2000.

[17] Z. Wang and X. Yang, "Ultra-wideband communications with blind channel estimation based on first-order statistics," *IEEE Signal Process. Lett.*, vol. 4, no. 5, pp. 529–532, May 2004.

[18] M. Z. Win and R. A. Scholtz, "Ultra wide bandwidth time-hopping spread-spectrum impulse radio for wireless multiple access communications," *IEEE Trans. Commun.*, vol. 48, no. 4, pp. 679–691, Apr. 2000.

[19] L. Yang and G. B. Giannakis, "Low-complexity training for rapid timing acquisition in ultra-wideband communications," in *Proc. Global Telecommun. Conf.*, San Francisco, CA, Dec. 1–5, 2003, pp. 769–773.

[20] ——, "Optimal pilot waveform assisted modulation for ultra-wideband communications," *IEEE Trans. Wireless Commun.*, vol. 3, no. 4, pp. 1236–1249, Jul. 2004.

[21] ——, "Ultra-wideband communications: An idea whose time has come," *IEEE Signal Process. Mag.*, vol. 21, no. 6, pp. 26–54, Nov. 2004.

[22] L. Yang, Z. Tian, and G. B. Giannakis, "Non-data aided timing acquisition of ultra-wideband transmissions using cyclostationarity," in *Proc. Int. Conf. Acoust., Speech, Signal Process.*, Hong Kong, China, Apr. 6–10, 2003, pp. 121–124.

[23] H. Zhang and D. L. Goeckel, "Generalized transmitted-reference UWB systems," in *Proc. Conf. Ultra-Wideband Syst. Technol.*, Reston, VA, Nov. 16–19, 2003, pp. 147–151.


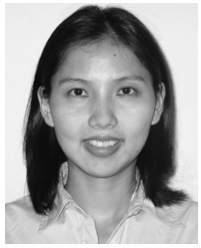

**Liuqing Yang** (M'04) received the B.S. degree in electrical engineering from Huazhong University of Science and Technology, Wuhan, China, in 1994, and the M.Sc. and Ph.D. degrees in electrical and computer engineering from the University of Minnesota, Minneapolis, in 2002 and 2004, respectively.

Since August 2004, she has been an Assistant Professor with the Department of Electrical and Computer Engineering, University of Florida, Gainesville. Her research interests include communications, signal processing, and networking. Currently, she has a particular interest in ultra-wideband communications. Her research encompasses synchronization, channel estimation, equalization, multiple access, space–time coding, and multicarrier systems.

**Georgios B. Giannakis** (F'97) received the Diploma in electrical engineering from the National Technical University of Athens, Athens, Greece, in 1981, and the MSc. degrees in electrical engineering in 1983 and mathematics in 1986, and the Ph.D. degree in electrical engineering in 1986 from the University of Southern California (USC), Los Angeles, CA,

After lecturing for one year at USC, he joined the University of Virginia in 1987, where he became a Professor of Electrical Engineering in 1997. Since 1999 he has been a Professor with the Department of Electrical and Computer Engineering, University of Minnesota, Minneapolis, where he now holds an ADC Chair in Wireless Telecommunications. His general interests span the areas of communications and signal processing, estimation and detection theory, time-series analysis, and system identification—subjects on which he has published more than 220 journal papers, 380 conference papers, and two edited books. Current research focuses on transmitter and receiver diversity techniques for single- and multiuser fading communication channels, complex-field and space–time coding, multicarrier, ultra-wideband wireless communication systems, cross-layer designs, and sensor networks.

Dr. Giannakis is the (co-) recipient of six paper awards from the IEEE Signal Processing (SP) and Communications Societies (1992, 1998, 2000, 2001, 2003, 2004). He received Technical Achievement Awards from the SP Society in 2000 and EURASIP in 2005. He served as Editor-in-Chief for the IEEE SIGNAL PROCESSING LETTERS, as Associate Editor for the IEEE TRANSACTIONS ON SIGNAL PROCESSING, and the IEEE SIGNAL PROCESSING LETTERS, as Secretary of the SP Conference Board, as Member of the SP Publications Board, as Member and Vice-Chair of the Statistical Signal and Array Processing Technical Committee, as Chair of the SP for Communications Technical Committee, and as a Member of the IEEE Fellows Election Committee. He has also served as a Member of the IEEE-SP Society's Board of Governors, the Editorial Board for the PROCEEDINGS OF THE IEEE, and the Steering Committee of the IEEE TRANSACTIONS ON WIRELESS COMMUNICATIONS.